Hydrido, Halo, and Hydrido-Halo Complexes of Two-Electron Mixed-Valence Diiridium Cores

Alan F. Heyduk and Daniel G. Nocera*

Contribution from the Department of Chemistry, 6-335, Massachusetts Institute of Technology, 77 Massachusetts Avenue Cambridge, Massachusetts 02139-4307

Received April 28, 2000

Abstract: Two-electron mixed-valence bimetallic cores of iridium are stabilized in a diphosphazane, MeN-$[P(OCH_2CF_3)_2]_2$ (bis(bis(trifluoroethoxy)phosphino)methylamine, tfepma) coordination sphere. Treatment of $[Ir(cod)Cl]_2$ with tfepma affords the $Ir_2^{0,II}$ complex, $Ir_2(tfepma)_3Cl_2$ (**1**), in which the Ir^0 and Ir^{II} centers assume trigonal bipyramidal and square pyramidal coordination geometries, respectively. The coordinatively unsaturated two-electron mixed-valence core of **1** supports an extensive acid−base and oxidation−reduction chemistry. As established by single crystal X-ray analysis, two-electron donor ligands are readily received at the Ir^{II} center of **1** to complete the octahedral coordination environment that is preferred by a d^7 metal−metal bonded center. Alternatively, redox-active substrates rapidly add across the single metal−metal bond of **1** to form $Ir_2^{I,III}$ mixed-valence complexes; the chlorine and hydrochloric acid adducts, $Ir_2(tfepma)_3Cl_4$ (**5**) and $Ir_2(tfepma)_3$-HCl_3 (**7b**), respectively, have been characterized by NMR spectroscopy and X-ray crystallography. Likewise, H_2 reacts with **1** to afford an $Ir_2^{I,III}$ dihydride complex, $Ir_2(tfepma)_3H_2Cl_2$ (**8**). Single-crystal X-ray and NMR analyses of **8** reveal that a single hydride ligand is coordinated at each iridium center of the bimetallic core. Hydrogen is readily removed from the complex in solution and the solid state, providing the first example of the reversible addition of dihydrogen across a single metal−metal bond.

Introduction

Mixed-valence complexes typically contain metals in formal oxidation states that differ by a single electron, which may localize within, or delocalize about, binuclear or polynuclear metal cores.[1−5] With a single electron defining the mixed-valence state, a common redox reaction of these complexes is one-electron exchange between M^n and M^{n+1} sites.[6−15] Net redox chemistry may be achieved when the M^n center promotes a one-electron reduction or, conversely, when the M^{n+1} center promotes a complementary one-electron oxidation.[16−20] Expanding on Taube's original construct of mixed valency,[21] we have turned our efforts to the synthesis and chemistry of two-electron mixed-valence complexes. Drawing a parallel to the one-electron reactivity of $M^n\cdots M^{n+1}$ species, we surmised that oxidation−reduction transformations promoted at the individual metal centers of two-electron mixed-valence bimetallic cores, $M^{n+1}\cdots M^{n-1}$ or $M^n\cdots M^{n+2}$, present the opportunity to develop novel multielectron chemistry.

A two-electron mixed-valence complex results when the metals of a symmetric bimetallic core can be induced to internally disproportionate. For $M^n\cdots M^n$ bimetallic cores featuring valence electrons in weakly coupled orbitals, this disproportionation may be accomplished by exciting metal-to-metal charge transfer (MMCT) transitions to give $M^{n+1}\cdots M^{n-1}$ electronic excited states. Such is the case for quadruply bonded metal−metal dimers. A lowest-energy electronic excited-state structure of zwitterionic parentage ($^+M—M:^-$) results from the promotion of an electron in the d_{xy} orbital localized on one center of the bimetallic core to the neighboring d_{xy} orbital, localized on the other metal center.[22−25] As anticipated for the reactivity

(1) Creutz, C. *Prog. Inorg. Chem.* **1983**, *30*, 1−73.
(2) Taube, H. In *Electron-Transfer Reactions: Inorganic, Organometallic and Biological Applications*; Isied, S. S., Ed.; Advances in Chemistry Series 253; American Chemical Society: Washington, DC, 1997; pp 1−17.
(3) Mouesca, J. M.; Lamotte, B. *Coord. Chem. Rev.* **1998**, *180*, 1573−1614.
(4) Gross, R.; Kaim, W. *Angew. Chem., Int. Ed. Engl.* **1987**, *26*, 251−253.
(5) *Mixed Valency System: Applications in Chemistry, Physics and Biology*; Prassides, K., Ed.; NATO ASI Series C: Mathematical and Physical Sciences 343; Kluwer Academic: Dordrecht, 1991.
(6) Schatz, P. N. In *Inorganic Electronic Structure and Spectroscopy*; Solomon, E. I., Lever, A. B. P., Eds.; Wiley-Interscience: New York, 1999; Vol. 2, pp 175−226.
(7) Brunschwig, B. S.; Sutin, N. *Coord. Chem. Rev.* **1999**, *187*, 233−254.
(8) Demadis, K. D.; El-Samanody, E. S.; Coia, G. M.; Meyer, T. J. *J. Am. Chem. Soc.* **1999**, *121*, 535−544.
(9) Ito, T.; Hamaguchi, T.; Nagino, H.; Yamaguchi, T.; Kido, H.; Zavarine, I. S.; Richmond, T.; Washington, J.; Kubiak, C. P. *J. Am. Chem. Soc.* **1999**, *121*, 4625−4632.
(10) Ito, T.; Hamaguchi, T.; Nagino, H.; Yamaguchi, T.; Washington, J.; Kubiak, C. P. *Science* **1997**, *277*, 660−663.
(11) Balzani, V.; Juris, A.; Venturi, M.; Campagna, S.; Serroni, S. *Chem. Rev.* **1996**, *96*, 759−833.
(12) Reimers, J. R.; Hush, N. S. *Inorg. Chim. Acta* **1994**, *226*, 33−42.
(13) Giuffrida, G.; Campagna, S. *Coord. Chem. Rev.* **1994**, *135*, 517−531.
(14) Kunkely, H.; Pawlowski, V.; Vogler, A. *Inorg. Chim. Acta* **1994**, *225*, 327−330.
(15) Vahrenkamp, H.; Geiss, A.; Richardson, G. N. *J. Chem. Soc., Dalton Trans.* **1997**, 3643−3651.
(16) Vogler, A.; Kunkely, H. *Top. Curr. Chem.* **1990**, *158*, 1−30.
(17) Vogler, A.; Osman, A. H.; Kunkely, H. *Coord. Chem. Rev.* **1985**, *64*, 159−173.
(18) Hennig, H. *Coord. Chem. Rev.* **1999**, *182*, 101−123.
(19) Scandola, F.; Indelli, M. T.; Chiorboli, C.; Bignozzi, C. A. *Top. Curr. Chem.* **1990**, *158*, 73−149.
(20) Sykora, J.; Sima, J. *Coord. Chem. Rev.* **1990**, *107*, 1−225.
(21) Taube, H. *Angew. Chem., Int. Ed. Engl.* **1984**, *23*, 329−339.
(22) Engebretson, D. S.; Zaleski, J. M.; Leroi, G. E.; Nocera, D. G. *Science* **1994**, *265*, 759−762.
(23) Engebretson, D. S.; Graj, E.; Leroi, G. E.; Nocera, D. G. *J. Am. Chem. Soc.* **1999**, *121*, 868−869.

10.1021/ja001491q CCC: $19.00
Published on Web 09/14/2000

of two-electron mixed-valence cores, this MMCT excited state promotes two-electron photoredox transformations involving quadruply bonded metal−metal complexes.[26−31] When a photon cannot be used to drive the formation of a two-electron mixed-valence intermediate, a ground-state $M^{n+2}\cdots M^{n}$ species must be stabilized relative to its symmetric $M^{n+1}\cdots M^{n+1}$ congener. Yet the paucity of molecular compounds displaying two-electron mixed-valence cores highlights the inability of common ligand systems to preferentially promote this internal disproportionation. Accordingly, the bis(difluorophosphino)methylamine (dfpma) ligand, $CH_3N(PF_2)_2$, is distinguished by its propensity to drive the conversion of binuclear $Rh^I(\mu\text{-}X)_2Rh^I$ (X = Cl, Br or I) dimers to two-electron mixed-valence $Rh_2^{0,II}$ complexes.[32,33] A high-resolution X-ray structure of the $Rh_2^{0,II}$ complex, $Rh_2(dfpma)_3Br_2(PPh_3)$ provides insight into the means by which the dfpma ligand accommodates an internally disproportionated metal core.[34] A pronounced asymmetry in the dfpma framework of the dirhodium complex suggests that the bridgehead N predominantly donates its lone pair to the PF_2 bonded to Rh^{II}; in the absence of $Rh^{II} \rightarrow PF_2$ π-back-bonding, the PF_2 group acts as a σ-donor to stabilize the high-valent Rh^{II} metal center. Correspondingly, with the N lone pair electron density channeled away from the neighboring PF_2 group, its strong π accepting properties are maintained and hence Rh^0 is stabilized. In this manner, we believe that the dfpma ligand is able to accommodate the intramolecular disproportionation of $Rh^I\cdots Rh^I$ to Rh^0-Rh^{II}.

The two-electron mixed valency of the Rh_2 dfpma system is unusual because it is not contingent on electron-counting formalisms. Octahedral Rh^{II} and trigonal bipyramidal Rh^0 centers compose a bimetallic core bridged by three dfpma ligands. Pairing the odd electron in the d_{z^2} orbital of the two 17 e^- Rh^0 and Rh^{II} centers leads to a formal metal−metal bond and a 36 e^- species. This formulation of two-electron mixed-valency is differentiated from the common structural motif that is exemplified by 34 e^- bimetallic compounds of cobalt, rhodium, and iridium.[35−39] Here, single-atom, anionic ligands such as chlorine, oxygen, or sulfur bridge 18 e^- octahedral and 16 e^- square planar metal centers of a binuclear metal core.[40] Depending on electron counting formalisms, these complexes may be described as two-electron mixed-valence species in which there is a dative $M^I \rightarrow M^{III}$ bond or, alternatively, as a symmetric 17 e^- species connected by a $M^{II}-M^{II}$ bond formed from the pairing of electrons from each of the metal centers.

By introducing the same dσ* excited state within the electronic structure of the LRh^0-Rh^0L, $LRh^0-Rh^{II}X_2$, and $X_2Rh^{II}-Rh^{II}X_2$ cores,[46] we have been able to interconvert between series members by the elimination of halogen in two-electron steps. Our success in effecting a four-electron photoredox chemistry among discrete molecular species[34,45] attests to the benefits gained from designing an authentic two-electron mixed-valence $Rh_2^{0,II}(dfpma)_3X_2L$ complex (X = Cl, Br and L = CO, PR_3, CNR), together with its reduced $Rh_2^{0,0}(dfpma)_3L_2$ and oxidized $Rh_2^{II,II}(dfpma)_3X_4$ partners. The mixed-valence compound is the linchpin that couples the two-electron M−X chemistry of the individual rhodium centers.

Because the high stabilities of metal−halide bonds prevent turnover in photocatalytic HX splitting cycles,[47−49] the ability to photoactivate M−X bonds from a two-electron mixed-valence platform is provocative from the standpoint of energy conversion considerations. To this end, we have become interested in defining the potential role of two-electron mixed-valence complexes in HX photocatalysis, necessitating a systematic understanding of the hydrido and hydrido−halo chemistry of this new class of compounds. The recent availability of the $Ir_2^{0,II}$ species, $Ir_2(tfepma)_3Cl_2$ (tfepma = $MeN[P(OCH_2CF_3)_2]_2$),[50] in consideration with the stability of third-row metal−hydride bonds, provides a heretofore unavailable opportunity to systematically investigate the hydrido and hydrido-halo coordination chemistry of two-electron mixed-valence complexes. As we now report, small molecule substrates H_2, Cl_2 and HCl readily react at the $Ir_2^{0,II}$ core to afford a set of structurally characterized complexes, which reveal an extensive oxidation−reduction chemistry for two-electron mixed-valence compounds, including the first example of reversible H_2 addition/elimination across a single metal−metal bond.

Experimental Section

General Considerations. All synthetic manipulations were conducted in the dry, anaerobic environment provided by a Schlenk-line or by a nitrogen-filled glovebox. Solvents for synthesis were reagent grade or better and were dried by following standard procedures.[51] Compounds gave satisfactory analyses, which were performed at H. Kolbe Mikroanalytisches Laboratorium.

Chlorine was delivered as the iodobenzene adduct, $PhICl_2$. The starting materials $[Ir(cod)Cl]_2$ (Strem), triethylsilane (Aldrich), triethylamine (Alfa-Aesar), 2,2,2-trifluoroethanol (Aldrich), methyliodide (Aldrich), trifluoromethanesulfonic acid (Alfa-Aesar), d^1-trifluoromethanesulfonic acid (Aldrich) and gaseous reactants, H_2 (BOC

(24) Cotton, F. A.; Nocera, D. G. *Acc. Chem. Res.* **2000**, *33*, 483−490.
(25) Hopkins, M. D.; Gray, H. B.; Miskowski, V. M. *Polyhedron* **1987**, *6*, 705−714.
(26) Partigianoni C. M.; Nocera, D. G. *Inorg. Chem.* **1990**, *29*, 2033−2034.
(27) Partigianoni, C. M.; Turró, C.; Hsu, T. L. C.; Chang I−J.; Nocera, D. G. In *Photosensitive Metal-Organic Systems: Mechanistic Principles and Applications*; Kutal, C., Serpone, N., Ed.; Advances in Chemistry Series 238; American Chemical Society: Washington, DC, 1993; pp 147−163.
(28) Nocera, D. G. *J. Cluster Sci.* **1994**, *5*, 185−209.
(29) Hsu, T. L. C.; Helvoigt, S. A.; Partigianoni, C. M.; Turró C.; Nocera, D. G. *Inorg. Chem.* **1995**, *34*, 6186−6190.
(30) Nocera, D. G. *Acc. Chem. Res.* **1995**, *28*, 209−217.
(31) Pistorio, B. J.; Nocera, D. G. *Chem. Commun.* **1999**, 1831−1832.
(32) Dulebohn, J. I.; Ward, D. L.; Nocera, D. G. *J. Am. Chem. Soc.* **1988**, *110*, 4054−4056.
(33) Dulebohn, J. I.; Ward, D. L.; Nocera, D. G. *J. Am. Chem. Soc.* **1990**, *112*, 2969−2977.
(34) Heyduk, A. F.; Macintosh, A. M.; Nocera, D. G. *J. Am. Chem. Soc.* **1999**, *121*, 5023−5032.
(35) McCollum, D. G.; Yap, G. P. A.; Rheingold, A. L.; Bosnich, B. *J. Am. Chem. Soc.* **1996**, *118*, 1365−1379.
(36) Schenck, T. G.; Downes, J. M.; Milne, C. R. C.; Mackenzie, P. B.; Boucher, H.; Whelan, J.; Bosnich, B. *Inorg. Chem.* **1985**, *24*, 2334−2337.
(37) Schenck, T. G.; Milne, C. R. C.; Sawyer, J. F.; Bosnich, B. *Inorg. Chem.* **1985**, *24*, 2338−2344.
(38) Hlatky, G. G.; Johnson. B. F. G.; Lewis, J.; Raithby, P. R. *J. Chem. Soc., Dalton Trans.* **1985**, 1277−1279.
(39) Cotton, F. A.; Kang, S.-J.; Mandal, S. K. *Inorg. Chim. Acta* **1993**, *206*, 29−39.
(40) For examples of complexes containing 16 e^- and 18 e^- centers that are not structurally butressed with a single atom bridge, see refs 41−44.
(41) Ling, S. S. M.; Jobe, I. R.; Manojloviæ-Muir, J.; Muir, K. W.; Puddephatt, R. J. *Organometallics* **1985**, *4*, 1198−1202.
(42) Ling, S. S. M.; Payne, N. C.; Puddephatt, R. J. *Organometallics* **1985**, *4*, 1546−1550.
(43) Jiang, F. M.; Male, J. L.; Biradha, K.; Leong, W. K.; Pomeroy, R. K.; Zaworotko, M. J. *Organometallics* **1998**, *17*, 5810−5819.
(44) Lagunas, M. C.; Gossage, R. A.; Spek, A. L.; van Koten, G. *Organometallics* **1998**, *17*, 731−741.
(45) Odom, A. L.; Heyduk, A. F.; Nocera, D. G. *Inorg. Chim. Acta* **2000**, *297*, 330−337.
(46) Kadis, J.; Shin, Y.-g. K.; Dulebohn, J. I.; Ward, D. L.; Nocera, D. G. *Inorg. Chem.* **1996**, *35*, 811−817.
(47) Gray, H. B.; Maverick, A. W. *Science* **1981**, *214*, 1201−1205.
(48) Roundhill, D. M.; Gray, H. B.; Che, C.-M. *Acc. Chem. Res.* **1989**, *22*, 55−61.
(49) Smith, D. C.; Gray, H. B. *Coord. Chem. Rev.* **1990**, *100*, 169−181.
(50) Heyduk, A. F.; Nocera, D. G. *Chem. Commun.* **1999**, 1519−1520.
(51) Armarego, W. L. F.; Perrin, D. D. *Purification of Laboratory Chemicals*, 4th ed.; Butterworth-Heinmann: Oxford, 1996.

Gases, UHP Grade 5), HCl, D_2, and DCl (Aldrich) were used as received. The ligand precursor $MeN(PCl_2)_2$,[52,53] and Ir^0-Ir^{II} compounds $Ir_2(tfepma)_3Cl_2(CNBu^t)$ (**2a**) and $Ir_2(tfepma)_3Cl_2(PEt_3)$ (**2b**)[50] were prepared by following published procedures.

General Methods. All NMR spectra were collected at the MIT Department of Chemistry Instrumentation Facility on a Varian Inova-Unity 500 Spectrometer unless otherwise noted. The NMR solvents C_6D_6, d^8-THF and CD_3CN (Cambridge Isotope Laboratories) were either dried using appropriate agents and degassed by at least three freeze−pump−thaw cycles, or used as received in glass ampules. ^1H NMR spectra (500 MHz) were referenced to TMS using the residual proteo impurities of the given solvent. $^{31}P\{^1H\}$ NMR spectra (202.5 MHz) were referenced to an external 85% H_3PO_4 standard. All chemical shifts are reported using the standard δ notation in parts-per-million; positive chemical shifts are to a higher frequency from the given reference. Rate constants for fluxional processes were calculated from VT NMR spectra using the Complete Bandshape Method; the corresponding activation parameters were calculated from Eyring plots.[54] IR spectra were recorded on a Nicolet Impact 410 spectrometer as either KBr pellets or Fluorolube mulls.

Preparation of tfepma. Although tfepma has been prepared previously,[55,56] we now describe a detailed synthesis of the bidentate diphosphazane. Dropwise addition of CF_3CH_2OH (36.8 g, 368 mmol, 4.25 equiv) to a −80 °C solution of triethylamine (36.49, 360 mmol, 4.16 equiv) and $MeN(PCl_2)_2$ (20.15 g, 86.56 mmol, 1 equiv) in 500 mL of diethyl ether results in a rapid and exothermic reaction, with concomitant formation of the white $[Et_3NH]Cl$ salt. After warming to room temperature, the mixture was stirred for 24 h. Filtration followed by rotary evaporation to remove ether afforded impure product as a clear, viscous liquid. Distillation under reduced pressure (75−85 °C, 0.5 Torr) was accompanied by some decomposition of the ligand, necessitating a second filtration to give 23.6 g (58% yield) of pure ligand. ^1H NMR (300 MHz, C_6D_6) δ/ppm: 2.506 (td, 3.898 Hz, 0.600 Hz, 3H), 3.55 (dp, 17.12 Hz, 4.4 Hz, 8H). $^{31}P\{^1H\}$ NMR (121.4 MHz, C_6D_6) δ/ppm: 148.614 (s). ^{19}F NMR (282 MHz, C_6D_6) δ/ppm: −76.90 (m).

Preparation of $Ir_2^{0,II}(tfepma)_3Cl_2$ (1). The iridium complex $Ir_2(tfepma)_3Cl_2$ (**1**),[50] previously prepared in our laboratories, is more conveniently synthesized as follows. Within the environs of a glovebox, $[Ir(cod)Cl]_2$ (2.06 g, 3.07 mmol, 1 equiv) was dissolved in 100 mL of toluene contained in a 250-mL Schlenk flask. To this solution, tfepma (4.63 g, 9.50 mmol, 3.1 equiv) in 10 mL of toluene was added dropwise, prompting a color change from orange to red. The flask was fitted with a reflux condenser and a nitrogen inlet, and then removed from the glovebox and attached to a Schlenk line. The mixture was heated to reflux for 1 h during which a dark solid formed. After cooling the mixture to room temperature, the toluene was removed by cannula filtration, and the solid was washed with 3 × 20 mL of pentane before drying under reduced pressure; **1** (4.5 g) was obtained in 77% yield as a green powder. The NMR features of **1** in CD_3CN at 25 °C have been previously reported; the data presented here are for solutions of **1** in d^8-THF at −80 °C. ^1H NMR (d^8-THF, −80 °C) δ/ppm: 2.61 (dd, 13.09 Hz, 10.59 Hz, 3H), 2.70 (s, 3H), 3.17 (s, 3H), 4.2−5.5 (m, 24H). $^{31}P-\{^1H\}$ NMR (d^8-THF, −80 °C) δ/ppm: 25.68 (s, 1P), 71.73 (ddt, 325.3 Hz, 297.6 Hz, 18.18 Hz, 1P), 78.31 (dm, 138.1 Hz, 1P), 89.76 (dd, 171.6 Hz, 39.26 Hz, 1P), 104.10 (dtdd, 326.7 Hz, 253.0 Hz, 137.3 Hz, 29.24 Hz, 1P), 106.12 (dtd, 296.6 Hz, 258.4 Hz, 170.3 Hz, 1P).

Dark green crystals of **1** are obtained by dissolving microcrystalline samples of the compound in a minimal amount of MeCN, diluting the resulting solution with CH_2Cl_2, filtering and layering the filtrate with an alkane solvent. Occasionally, a small crop of large yellow crystals (**3**) would coprecipitate from solution. The ^{31}P NMR spectra of the green-brown crystals of **1** and the yellow crystals of **3** dissolved in CD_3CN are identical; however, the ^1H NMR spectrum of **3** shows an additional peak at 1.963 ppm, attributed to approximately one equivalent of uncoordinated proteo MeCN.

Reaction of 1 with Bu_4NBr. A 0.7-mL CD_3CN solution of **1** (100 mg, 0.052 mmol, 1 equiv) was treated with 23 mg of Bu_4NBr (0.071 mmol, 1.4 equiv). As the Bu_4NBr dissolved, the solution color turned from brown to orange. ^1H and ^{31}P NMR spectroscopy established the quantitative conversion of **1** to $[Ir_2(tfepma)BrCl_2]^-$ (**2c**). ^1H NMR (CD_3CN) δ/ppm: 0.961 (t, 7.39 Hz, 12H), 1.352 (dq, 15.0 Hz, 7.38 Hz, 8H), 1.604 (m, 8H), 3.109 (m, 9H), 4.2−6.0 (m, 24H). $^{31}P\{^1H\}$ NMR (CD_3CN) δ/ppm: 35.015 (s, 1P), 41.074 (t, 303 Hz, 1P), 70.748 (t, 70.6 Hz, 2P), 98.240 (dm, 308 Hz, 2P).

Reaction of 1 with Triflic Acid. An NMR tube was charged with **1** (74 mg, 0.039 mmol, 1 equiv) in 0.7 mL of CD_3CN. The solution was treated with 34 μl of HOTf (OTf = OSO_2CF_3) (0.39 mmol of HOTf, 10 equiv), delivered via autopipet. Upon mixing, the solution turned pale yellow to quantitatively give $[HIr_2(tfepma)_3Cl_2(MeCN)]$-OTf (**4**). Alternatively, treatment of a suspension of **1** (192 mg, 0.100 mmol, 1 equiv) in 9 mL of CH_2Cl_2 with HOTf (20 mg, 0.13 mmol, 1.3 equiv) in 1 mL of MeCN caused all solid to dissolve, giving a very pale yellow solution. Precipitation of an eggshell solid was aided by the addition of 10 mL of pentane, affording 163 mg (77%) of **4**. ^1H NMR (CD_3CN) δ/ppm: −12.669 (m, 1H), 1.964 (s, see text), 2.586 (d, 1 Hz, see text), 2.728 (t, 11.5 Hz, 3H), 2.865 (dd, 8.84 Hz, 7.53 Hz, 3H), 3.092 (t, 7.86 Hz, 3H), 4.1−5.3 (m, 24H). $^{31}P\{^1H\}$ NMR (CD_3CN) δ/ppm: 43.007 (dd, 744 Hz, 35.3 Hz, 1P), 48.383 (ddt, 716 Hz, 45.6 Hz, 17.9 Hz, 1P), 53.628 (dd, 147 Hz, 38.0 Hz, 1P), 66.898 (dd, 150 Hz, 39.3 Hz, 1P), 75.931 (ddt, 739 Hz, 148 Hz, 39.7 Hz, 1P), 84.947 (ddt, 722 Hz, 146 Hz, 34.9 Hz 1P). IR (Fluorolube) ν_{Ir-H}/cm^{-1}: 2042.

Reaction of 1 with $PhICl_2$ to $Ir_2^{I,III}(tfepma)_3Cl_4$ (5). $PhICl_2$ (20 mg, 0.073 mmol, 1.3 equiv) in 2 mL of CH_2Cl_2 was added to an 8-mL CH_2Cl_2 suspension of **1** (105 mg, 0.055 mmol, 1 equiv). As **1** reacts, the suspension is brought into solution, which turns bright yellow and a yellow solid subsequently forms. To ensure complete reaction, stirring was continued at room temperature for 2 h after the onset of precipitation. Addition of pentane followed by filtration gave 54 mg (37% yield) of a bright yellow powder. Single crystals of **5** were grown from saturated solutions of the complex in CH_2Cl_2, layered with heptane. Anal. Calcd for $C_{27}H_{33}Cl_4F_{36}Ir_2N_3O_{12}P_6$: C, 16.32; H, 1.67; N, 2.11; P, 9.35. Found: C, 16.37: H, 1.78; N, 2.09; P, 9.40. ^1H NMR (CD_3CN) δ/ppm: 2.71 (t, 8.40 Hz, 3H), 2.87 (t, 9.38 Hz, 3H), 2.93 (t, 7.78 Hz, 3H), 4.3−4.6 (m, 6H), 4.7−5.1 (m, 12H), 5.40 (ddqd, 179.6 Hz, 12.14 Hz, 8.80 Hz, 2.93 Hz, 2H), 5.91 (ddq, 151.1 Hz, 12.20 Hz, 8.81 Hz, 2H). $^{31}P\{^1H\}$ NMR (CD_3CN) δ/ppm: 9.24 (dt, 80.50 Hz, 25.86 Hz, 1P), 13.14 (ddd, 900.7 Hz, 79.93 Hz, 31.16 Hz, 1P), 54.98 (dt, 136.2 Hz, 29.08 Hz, 1P), 57.11 (dt, 125.6 Hz, 28.48 Hz, 1P), 66.46 (dt, 124.5 Hz, 30.50 Hz, 1P), 74.31 (ddd, 900.8 Hz, 136.6 Hz, 30.89 Hz, 1P).

Preparation of $Ir_2^{II,II}(tfepma)_2Cl_4(MeCN)_2$ (6). A solution of **1** (150 mg, 0.078 mmol, 1 equiv) and $PhICl_2$ (150 mg, 0.50 mmol, 6 equiv) in 10 mL CH_3CN was heated to reflux for 48 h. The solvent was removed under reduced pressure, and the residue was taken up in 5 mL of CH_2Cl_2. The solution was filtered and then concentrated to 2 mL by vacuum distillation. Addition of a 10-mL aliquot of pentane caused 100 mg (81% yield) of **6** to precipitate as a yellow powder, which was collected and dried in vacuo. Single crystals of **6** were grown by layering saturated CH_2Cl_2 solutions of the complex with heptane. Anal. Calcd for $C_{22}H_{28}Cl_4F_{24}Ir_2N_4O_8P_4$: C, 16.70; H, 1.78; N, 3.54. Found: C, 16.58: H, 1.88; N, 3.52. ^1H NMR (CD_3CN) δ/ppm: 2.80 (t, 8.13 Hz, 6H), 4.48 (q, 2.93 Hz, 4H), 4.6−4.8 (m, 4H), 4.95−5.15 (m, 6H), 5.46 (dqd, 12.31 Hz, 8.93 Hz, 3.62 Hz, 2H). $^{31}P\{^1H\}$ NMR (CD_3CN) δ/ppm: 54.97 (dd, 121.4 Hz, 42.41 Hz, 2P), 57.87 (dd, 121.4 Hz, 41.64 Hz, 2P).

Reaction of 1 with HCl to $Ir_2(tfepma)_3HCl_3$ (7a and 7b). A suspension of **1** (120 mg, 0.063 mmol) in 10 mL of CH_2Cl_2 was purged with HCl gas. Within 5 min, all solid had dissolved to give a yellow solution. Immediate solvent removal gave 131 mg (97% yield) of **7a** with an empirical formula $Ir_2(tfepma)_3HCl_3$. Anal. Calcd for $C_{27}H_{34}Cl_3F_{36}Ir_2N_3O_{12}P_6$: C, 16.60; H, 1.75; N, 2.15; P, 9.52. Found: C, 16.57: H, 1.84; N, 2.08; P, 9.68. ^1H NMR (CD_3CN) δ/ppm: −12.985 (m, 1H), 2.757 (t, 11.2 Hz, 3H), 2.916 (s, 6H), 4.0−5.9 (m, 24H). $^{31}P-$

(52) Nixon, J. F. *J. Chem. Soc. A* **1968**, 2689−2692.
(53) King, R. B.; Gimeno, J. *Inorg. Chem.* **1978**, *17*, 2390−2395.
(54) Sandström, J. *Dynamic NMR Spectroscopy*; Academic Press: London, 1982.
(55) Ganesan, M.; Krishnamurthy, S. S.; Nethaji, M. *J. Organomet. Chem.* **1998**, *570*, 247−254.
(56) Balakrishna, M. S.; Prakasha, T. K.; Krishnamurthy, S. S.; Siriwardane, U.; Hosmane, N. S. *J. Organomet. Chem.* **1990**, *390*, 203−16.

{^{1}H} NMR (CD_3CN) δ/ppm: 35.712 (ddd, 795 Hz, 44 Hz, 18.9 Hz, 1P), 47.878 (dd, 752 Hz, 49 Hz, 1P), 63.794 (dd, 147 Hz, 34 Hz, 1P), 66.339 (dd, 146 Hz, 35 Hz, 1P), 80.880 (dddd, 795 Hz, 146 Hz, 54 Hz, 29 Hz, 1P), 88.657 (dddd, 751 Hz, 147 Hz, 44 Hz, 29 Hz, 1P). IR (KBr) ν_{Ir-H}/cm^{-1}: 2037.

When solvent was not immediately removed, and the solution was stirred for 24 h at room temperature, a very pale yellow solid precipitated from solution. NMR analysis of this solid in CD_3CN revealed the formation of an isomer of $Ir_2(tfepma)_3HCl_3$, **7b**, in 68% isolated yield. The preparation of **7b** on a larger scale proceeds smoothly by treating a suspension of **1** (1.153 g, 0.6016 mmol) in 150 mL of CH_2Cl_2 with HCl gas for 10 min. The flask headspace was purged with N_2, and the solution was stirred for 24 h. The volume of the mixture was reduced to ~40 mL by distillation under reduced pressure. Addition of 60 mL of pentane facilitated the precipitation of 640 mg (54%) of analytically pure **7b**, which was washed with pentane and dried in vacuo. Single crystals of this complex are readily obtained by layering a CH_2Cl_2 solution of **7b** with heptane. Anal. Calcd for $C_{27}H_{34}Cl_3F_{36}Ir_2N_3O_{12}P_6$: C, 16.60; H, 1.75; N, 2.15; P, 9.52. Found: C, 16.47: H, 1.74; N, 2.15; P, 9.58. ^{1}H NMR (CD_3CN) δ/ppm: −10.261 (ddt, 178 Hz, 18.2 Hz, 12.2 Hz, 1H), 2.65 (t, 10.84 Hz, 3H), 2.77 (t, 7.49 Hz, 3H), 2.89 (t, 7.74 Hz, 3H), 4.1−5.1 (m, 21H), 5.3−5.5 (m, 1H), 5.7−6.1 (m, 2H). ^{31}P{^{1}H} NMR (CD_3CN) δ/ppm: 21.64 (tp, 34.17 Hz, 21.68 Hz, 1P), 26.61 (dtd, 761.5 Hz, 33.05 Hz, 10.27 Hz, 1P), 64.38 (dddd, 130.6 Hz, 35.66 Hz, 21.52 Hz, 10.06 Hz, 1P), 67.79 (ddd, 162.2 Hz, 36.45 Hz, 19.99 Hz, 1P), 82.15 (dddd, 760.1 Hz, 130.8 Hz, 22.02 Hz, 13.08 Hz, 1P), 86.40 (dm, 162.6 Hz, 1P). IR (KBr) ν_{Ir-H}/cm^{-1}: 2115.

Reaction of 1 with H_2 to $Ir_2^{I,III}(tfepma)_3H_2Cl_2$ (8). Dihydrogen was bubbled slowly into a 10-mL CH_2Cl_2 suspension of **1** (76 mg, 0.040 mmol). The solid dissolved immediately to give a yellow solution, which returned to brown with concomitant formation of solid upon purging with N_2. Treating with H_2 regenerated the yellow solution. The solution could be cycled reversibly between yellow and brown with treatment of H_2 and N_2, respectively. The reaction proceeds with equal facility in CD_3CN. Integration of the ^{1}H NMR spectra obtained on solutions before and after H_2 addition indicates a quantitative reaction. A pale yellow solid is isolated when CH_2Cl_2 solutions were concentrated under a stream of H_2 to a few mLs, followed by pentane addition and cooling to −80 °C. An accurate yield and elemental analysis of the compound could not be determined because the complex loses H_2 in an atmosphere devoid of dihydrogen. The reaction is so prevalent that it occurs even in the solid-state, thus requiring us to grow X-ray quality single crystals of the complex from a CH_2Cl_2 solution of **8** layered with octane under a dihydrogen atmosphere. ^{1}H NMR (CD_3CN) δ/ppm: −11.626 (dq, 188 Hz, 16.0 Hz, 1H), −8.174 (d, 278 Hz, 1H), 2.81 (t, 6.72 Hz, 3H), 2.82 (t, 7.37 Hz, 6H), 4.2−5.7 (m, 24 H). ^{31}P{^{1}H} NMR (CD_3CN) δ/ppm: 17.85 (s, 1P), 45.26 (d, 746 Hz, 1P), 71.34 (d, 159 Hz, 1P), 86.84 (d, 155 Hz, 1P), 95.50 (dd, 752 Hz, 218 Hz, 1P), 99.40 (d, 222 Hz, 1P). IR (KBr) ν_{Ir-H}/cm^{-1}: 2053, 2071.

General Details of X-ray Data Collection and Reduction. X-ray diffraction data were collected on a Siemens 3-circle platform diffractometer equipped with a CCD detector. Measurements were carried out at −90 °C using Mo Kα (λ = 0.71073 Å) radiation, which was wavelength selected with a single-crystal graphite monochromator. Four sets of data were collected using ω scans and a −0.3° scan width. All calculations were performed on a Silicon Graphics Indigo 2 workstation. The data frames were integrated to *hkl*/intensity, and final unit cells were calculated by using the SAINT program v4.050 from Siemens. The structures were solved and refined with the SHELXTL v5.03 suite of programs developed by G. M. Sheldrick and Siemens Industrial Automation, Inc, 1995.

X-ray Structure of $[Ir_2(tfepma)_3Cl_2(MeCN)]\cdot MeCN$ (3·MeCN). A 0.24 mm × 0.32 mm × 0.32 mm fragment of a yellow crystal was excised from a larger crystal, which was obtained by vapor diffusing pentane into a CH_2Cl_2/MeCN solution of **1**. The crystal was coated in Paratone N and mounted onto a glass fiber. A total of 25467 reflections were collected in the θ range of 2.43° to 23.31°, of which 9155 were unique (R_{int} = 0.0313). The structure was solved by the Patterson heavy atom method in conjunction with standard difference Fourier techniques. Fluorine atoms of the $-CF_3$ groups were placed in ideal positions and refined as a rigid group before being allowed to refine freely in the final refinement cycles. Hydrogen atoms were placed in calculated positions using a standard riding model and they were refined isotropically. The orientation of the uncoordinated MeCN solvent molecule was assigned arbitrarily as the difference between the carbon and nitrogen terminus could not be definitively established. The largest peak and hole in the difference map were 0.754 and −0.470 eÅ^{-3}, respectively. The least squares refinement converged normally giving residuals of R1 = 0.0287, wR2 = 0.0709, and GOF = 1.021. The crystal data for $C_{31}H_{49}Cl_2F_{36}Ir_2N_5O_{12}P_6$: orthorhombic, $P2_12_12_1$, Z = 4, a = 13.078(6) Å, b = 17.505(9) Å, c = 27.837(14) Å, V = 6373(5) Å^3, ρ_{calc} = 2.083 g/cm^3, F(000) = 3832.

X-ray Structure of $[Ir_2(tfepma)_3Cl_4]_2\cdot CH_2Cl_2$ (5·CH_2Cl_2). A 0.32 mm × 0.10 mm × 0.08 mm yellow crystal of plate morphology was obtained by layering a CH_2Cl_2 solution of **5** with heptane. The crystal was coated in Paratone N and mounted onto a glass fiber. A total of 51168 reflections were collected in the θ range of 1.24° to 23.25°, of which 18252 were unique (R_{int} = 0.0955). The structure was solved by the Patterson heavy atom method in conjunction with standard difference Fourier techniques. Fluorine atoms were placed in ideal positions and subsequently allowed to refine freely. Hydrogen atoms were placed in calculated positions using a standard riding model and were refined isotropically. Two crystallographically unique but chemically identical iridium molecules were found in the asymmetric unit. The largest peak and hole in the difference map were 1.456 and −1.216 eÅ^{-3}, respectively. The least squares refinement converged normally giving residuals of R1 = 0.0803, wR2 = 0.1363, and GOF = 1.145. The crystal data for $C_{27.50}H_{34}Cl_5F_{36}Ir_2N_3O_{12}P_6$: monoclinic, $P2_1/c$, Z = 8, a = 23.6253(3) Å, b = 24.3565(4) Å, c = 24.93500(10) Å, β = 116.5400(10)°, V = 12836.3(3) Å^3, ρ_{calc} = 2.101 g/cm^3, F(000) = 7752.

X-ray Structure of $[Ir_2(tfepma)_2Cl_4(MeCN)_2]_2$ (6). A 0.50 mm × 0.20 mm × 0.08 mm yellow crystal of plate morphology was obtained by layering a CH_2Cl_2 solution of **6** with heptane. The crystal was coated in Paratone N and mounted onto a glass fiber. A total of 20933 reflections were collected in the θ range of 1.27° to 23.26°, of which 14281 were unique (R_{int} = 0.0419). The structure was solved by the Patterson heavy atom method in conjunction with standard difference Fourier techniques. Fluorine atoms were placed in ideal positions and subsequently allowed to refine freely. Hydrogen atoms, placed in calculated positions using a standard riding model, were refined isotropically. Again, as in **5**, two crystallographically unique but chemically identical iridium molecules were found in the asymmetric unit. The largest peak and hole in the difference map were 1.484 and −1.235 eÅ^{-3}, respectively. The least squares refinement converged normally giving residuals of R1 = 0.0749, wR2 = 0.1598, and GOF = 1.144. The crystal data for $C_{22.50}H_{29}Cl_5F_{24}Ir_2N_4O_8P_4$: triclinic, $P\bar{1}$, Z = 4, a = 16.5448(11) Å, b = 16.5925(11) Å, c = 19.2595(13) Å, α = 96.1220(10)°, β = 90.0930(10)°, γ = 104.0800(10)°, V = 5096.9(6) Å^3, ρ_{calc} = 2.118 g/cm^3, F(000) = 3084.

X-ray Structure of $Ir_2(tfepma)_3HCl_3\cdot CH_2Cl_2$ (7b·CH_2Cl_2). A 0.75 mm × 0.75 mm × 0.50 mm yellow crystal of plate morphology was obtained by layering a CH_2Cl_2 solution of **7b** with heptane. The crystal was coated in Paratone N and mounted onto a glass fiber. A total of 24906 reflections were collected in the θ range of 1.40° to 23.26°, of which 8802 were unique (R_{int} = 0.0414). The structure was solved by the Patterson heavy atom method in conjunction with standard difference Fourier techniques. The iridium-coordinated hydrogen was located in the difference Fourier map after all non-hydrogen atoms were located; the hydride was subsequently refined using a fixed Ir−H distance of 1.4 Å. All other hydrogen atoms were placed in calculated positions using a standard riding model and were refined isotropically. The largest peak and hole in the difference map were 1.286 and −0.927 eÅ^{-3}, respectively. The least squares refinement converged normally giving residuals of R1 = 0.0297, wR2 = 0.0711, and GOF = 1.102. The crystal data for $C_{28}H_{36}Cl_5F_{36}Ir_2N_3O_{12}P_6$: monoclinic, $P2_1/n$, Z = 4, a = 12.8111(2) Å, b = 17.0106(2) Å, c = 28.46680(10) Å, β = 99.2430(10)°, V = 6123.06(12) Å^3, ρ_{calc} = 2.211 g/cm^3, F(000) = 3896.

X-ray Structure of $Ir_2(tfepma)_3H_2Cl_2\cdot CH_2Cl_2$ (8·CH_2Cl_2). A 0.50 mm × 0.50 mm × 0.25 mm crystal fragment was taken from a larger yellow crystal of plate morphology, obtained by layering a CH_2Cl_2 solution of **8** with heptane under an H_2 atmosphere. The crystal was

coated in Paratone N and mounted onto a glass fiber. A total of 19041 reflections were collected in the θ range of 1.24° to 23.27°, of which 8475 were unique ($R_{int} = 0.0721$). The structure was solved by the Patterson heavy atom method in conjunction with standard difference Fourier techniques. The Ir^{I}-coordinated hydrogen was located in the difference Fourier map after assignment of all non-hydrogen atoms; it was subsequently refined using a fixed Ir−H distance of 1.4 Å. The Ir^{III}-coordinated hydrogen was placed in a vacant coordination site of the Ir^{III} center, with an Ir−H bond distance of 1.4 Å. All other hydrogen atoms were placed in calculated positions using a standard riding model and were refined isotropically. The largest peak and hole in the difference map were 1.862 and −1.708 eÅ^{-3}, respectively. The least squares refinement converged normally giving residuals of R1 = 0.0539, wR2 = 0.1299, and GOF = 1.210. The crystal data for $C_{28}H_{37}Cl_4F_{36}Ir_2N_3O_{12}P_6$: monoclinic, $P2_1/n$, $Z = 4$, $a = 10.9265(3)$ Å, $b = 24.1981(7)$ Å, $c = 22.6237(7)$ Å, $\beta = 97.1060(10)°$, $V = 5935.8(3)$ Å^3, $\rho_{calc} = 2.242$ g/cm^3, $F(000) = 3832$.

Extended Hückel Calculations. Electronic structure calculations were performed on a Silicon Graphics Indy workstation using the YAeHMOP software, v2.0.[57] The molecular structure of complex **1** was approximated as the idealized molecule, $Ir_2(PH_3)_6Cl_2$. Iridium−ligand bond lengths and angles for the complex were taken from the crystal structure of **1**. The input files are available as Supporting Information. Graphic representations of the metal-based HOMO and LUMO for each molecule were generated from the Viewkel output of the YAeMOP calculation and subsequently modified with the ray-tracing program Rayshade.[58]

Results

Simple Addition Reactions to the $Ir_2^{0,II}Cl_2$ Core. The two-electron mixed-valence $Ir_2^{0,II}$ core was unknown previous to the coordination chemistry of tfepma (tfepma = MeN[P(OCH$_2$CF$_3$)$_2$]$_2$). The bidentate diphosphazane ligand is prepared by the addition of CF_3CH_2OH to cold Et_2O solutions of $MeN(PCl_2)_2$ and NEt_3. We have recently communicated the reaction of tfepma with $[Ir(cod)Cl]_2$ to produce $Ir_2^{0,II}(tfepma)_3Cl_2$ (**1**) in moderate to good yields.[50] As summarized in Scheme 1 (only the PNP backbones of the ligands are depicted), the coordination sphere of the $Ir_2^{0,II}$ tfepma complex is distinguished from its $Rh_2^{0,II}$ dfpma counterpart by the preference of one bidentate ligand to chelate rather than bridge the bimetallic core. With the phosphorus of the chelating diphosphazane axially ligating Ir^0, the terminal donor ligand of the rhodium complex is not required. In turn, the absence of a third phosphorus ligand in the equatorial plane of Ir^{II} demands the equatorial coordination of two halides to the Ir^{II} center, leaving its axial coordination site vacant.

The coordinative unsaturation of **1** is the basis for an extensive reaction chemistry. Two-electron donor ligands such as *tert*-butylisonitrile (**2a**), triethylphosphine (**2b**) and bromide (**2c**) are readily received at the vacant Ir^{II} axial site of **1**, conferring the octahedral coordination geometry that is preferred by a d^7 metal center. As is apparent in the ORTEP of the $CNBu^t$ complex (**2a**) shown in Figure 1, the $Ir_2^{0,II}$ mixed-valence core is preserved upon axial ligation. Apart from changes along the $P_{ax}-Ir^0-Ir^{II}-L_{ax}$ axis, the X-ray crystal structure of **2a** is largely undistinguished from that of **1**.[50] In agreement with the solid-state results, the integration ratios for the proton resonances of L_{ax} to those of tfepma establish that only one donor ligand is incorporated into the diiridium coordination sphere. Moreover, room-temperature NMR spectra of **2a**−**c** in CD_3CN reveal static solution structures that are also consistent with the results of

Scheme 1

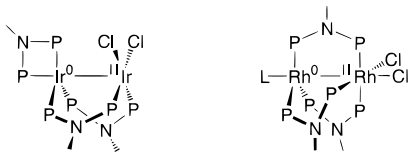

X-ray crystallography. Notably, the Ir^{II}-coordinated phosphites of **2a**, **2b**, and **2c** give rise to sharp triplet signals in the $^{31}P\{^1H\}$ NMR spectrum (Supporting Information, Figure S1) at 72.5, 66.0, and 70.7 ppm, respectively. The absence of fluxional behavior is also in evidence from the sharp high frequency doublet resonances of the Ir^0-coordinated phosphites of the bridging ligands. Whereas the ^{31}P resonances of the equatorial phosphites coordinated to the Ir^0 center in **1** and **2** are virtually identical, the ^{31}P resonance of the axial phosphite of the chelating diphosphazane shifts in accordance with the structural perturbations induced by the presence of a donor ligand in the axial coordination site of Ir^{II}. The observed increase in the Ir^0-P_{ax} bond distance ($d(Ir^0-P_{ax}) = 2.238(6)$ Å in **2a** vs $d(Ir^0-P_{ax}) = 2.206(4)$ Å in **1**) upon coordination of the donor ligand decreases $Ir^0 \rightarrow P_{ax}$ π-back-bonding, thus accounting for the pronounced high-frequency shift of the axial phosphite resonance. A sizable $^3J_{P_{ax}}-PEt_3$ coupling (e.g., 207 Hz for **2b**), and its absence in **1**, follows logically from the coordination of a phosphorus donor ligand along the metal−metal bond.

When the two-electron donor ligand is only weakly coordinating, the arrangement of the donor and halide ligands of the octahedral Ir^{II} changes in the manner shown by the X-ray crystal structure of the acetonitrile adduct (**3**) presented in Figure 1. Table 1 lists selected metrical parameters for the structure. Although the coordination mode of the tfepma ligands in **3** is unaltered from that observed in **2**, the coordination positions of a halide and the axial donor ligand are interchanged. The weakly coordinating MeCN ligand readily undergoes solvent exchange as revealed by the appearance of a resonance for uncoordinated proteo MeCN at 1.93 ppm in the ^1H NMR spectrum of **3** in CD_3CN. All other resonances in the ^1H NMR spectrum of **3** are identical to those observed in the spectrum of **1**.

The solvent exchange process of **1** was examined in CD_3CN and d^8-THF by variable temperature ^1H and ^{31}P NMR spectroscopy. Figure 2 presents ^1H and ^{31}P NMR spectra for the stopped-exchange and near-fast exchange limits in THF; similar results are obtained in CD_3CN solution. At room temperature, the NMR spectra of **1** and **3** are consistent with the X-ray structure of the former. Namely, a methyl resonance at 2.62 ppm, assigned to the chelating ligand, and a broad resonance at 2.91 ppm, assigned to the bridging ligands, are present at the expected 1:2 ratio. Upon cooling below −25 °C, NMR spectra of both complexes are identical and consonant with the asymmetric coordination environment displayed in the X-ray crystal structure of **3**. The broad resonance at 2.91 ppm splits into two singlets, indicative of different environments for the bridging tfepma ligands. The 24 protons attributed to the methylene resonances of the diphosphazane's OCH_2CF_3 groups (not shown in Figure 2) are not well resolved at any temperature.

A similar trend is observed in the ^{31}P NMR spectra of **1** and **3**. Below the coalescence temperature, spectra of **1** and **3** are identical and congruent with the solid-state structure of **3**. The two low-frequency resonances at 25.7 and 71.7 ppm are assigned to the chelating tfepma ligand, with the axial phosphite appearing at lowest frequency. The remaining resonances are due to the bridging tfepma ligands. Two overlapping high-

(57) Landrum, G. A.; YAeHMOP: Yet Another extended Hückel Molecular Orbital Package. YAeHMOP is freely available at http://overlap.chem.cornell.edu: 8080/yaehmop.html.

(58) Kolb, C.; Bogart, R.; Rayshade, v. 4.0; Rayshade is available at http://aperture.stanford.edu/~cek/rayshade/rayshade.html.

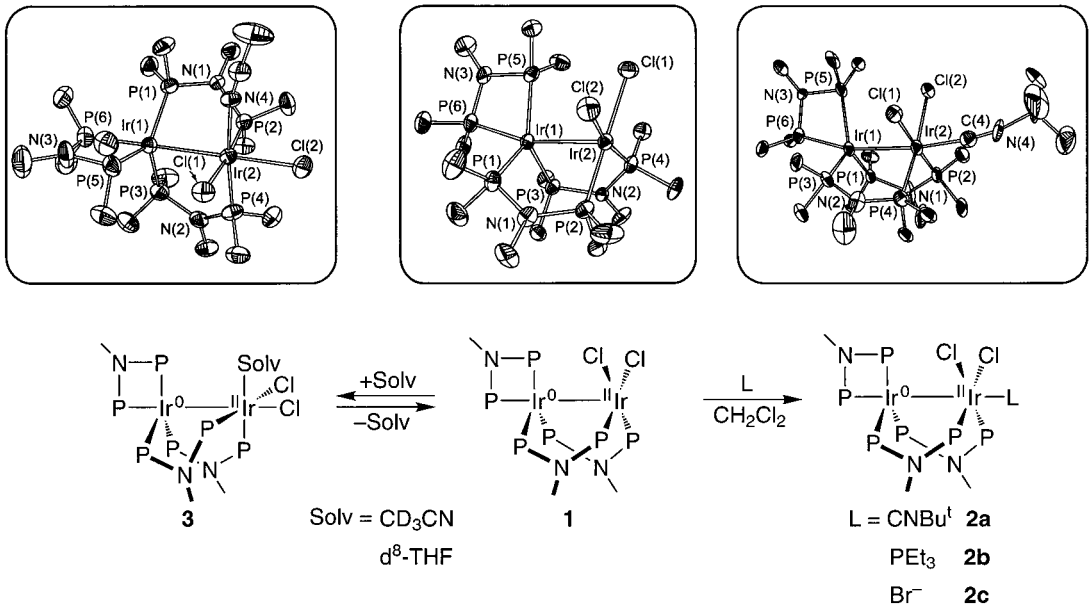

Figure 1. Reaction chemistry of $Ir_2(tfepma)_3Cl_2$ (**1**) with two-electron donor ligands. Thermal ellipsoid plots of the crystal structures are drawn at the 50% probability level and the numbering scheme is shown. Solvent molecules and $-CH_2CF_3$ groups are omitted for clarity.

Table 1. Selected Crystallographic Bond Distances (Å) and Angles (deg) for the Complexes **1** and **3**[a]

	bond lengths/Å	
	1	**3**
Ir(1)—Ir(2)	2.7871(8)	2.7963(11)
Ir(1)—P(1)	2.236(4)	2.217(2)
Ir(1)—P(3)	2.268(4)	2.225(2)
Ir(1)—P(5)	2.272(4)	2.272(2)
Ir(1)—P(6)	2.206(4)	2.227(2)
Ir(2)—Cl(1)	2.375(4)	2.427(2)
Ir(2)—Cl(2)	2.363(4)	2.513(2)
Ir(2)—P(2)	2.192(4)	2.186(2)
Ir(2)—P(4)	2.189(4)	2.176(2)
Ir(2)—N(4)	N/A	2.120(7)
	bond angles/deg	
	1	**3**
P(1)—Ir(1)—P(3)	106.8(2)	117.06(8)
P(1)—Ir(1)—P(5)	136.8(2)	128.93(9)
P(2)—Ir(2)—P(4)	96.2(2)	92.54(8)
P(2)—Ir(2)—Cl(1)	172.8(2)	173.16(7)
P(2)—Ir(2)—Cl(2)	88.2(2)	99.31(7)
Ir(2)—Ir(1)—P(6)	164.02(12)	165.26(7)
Ir(1)—Ir(2)—Cl(2)	104.52(11)	174.72(5)
P(2)—Ir(2)—N(4)		89.46(18)

[a] The data for **1** are taken from the previously published structure.[50]

frequency resonances (100−110 ppm) arise from the Ir^0-coordinated phosphites and the resonances at 78.3 and 89.8 ppm arise from the phosphites coordinated to the Ir^{II} center. As temperature is increased, solvent exchange permutes the phosphite signals of the bridging tfepma ligands. The Ir^{II}-bound phosphites exhibit the more pronounced coalescence behavior, consistent with solvent exchange occurring at the Ir^{II} center.

Rate constants for the exchange process were determined by monitoring the ^1H methyl resonances of the bridging tfepma of **1** or **3** in d^8-THF over the temperature range of −70 to +30 °C. Analysis of the Eyring plot, provided as Figure S3 in Supporting Information, yields activation parameters of $\Delta H^‡ = 13 \pm 1$ kcal mol^{-1} and $\Delta S^‡ = 6.6 \pm 2$ cal mol^{-1} K^{-1}. CD_3CN affords a narrower temperature range (−5 °C to 30 °C) over which an Eyring plot may be constructed (Supporting Information, Figure S3); activation parameters measured for this solvent system are $\Delta H^‡ = 25 \pm 4$ kcal mol^{-1} and $\Delta S^‡ = 38 \pm 5$ cal mol^{-1} K^{-1}. The positive activation entropies in both solvent systems comply with a dissociative process.[59] As $\Delta H^‡$ for a dissociative process is reflective of the metal−ligand bond strength,[60] the higher observed activation enthalpy for MeCN exchange follows directly from the greater tenacity of acetonitrile (as compared to THF) for late transition metals.

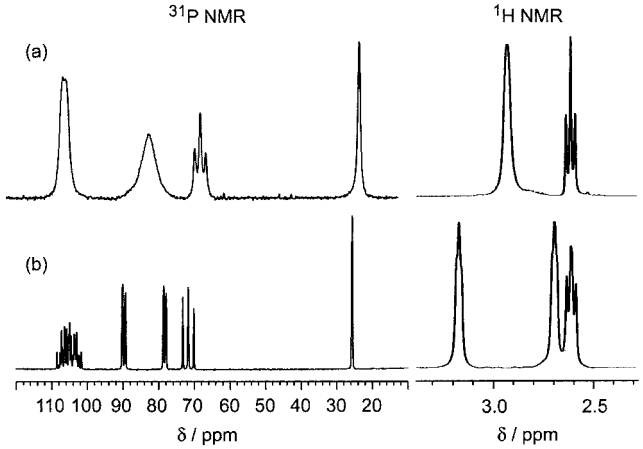

Figure 2. ^1H (partial) and $^{31}P\{^1H\}$ NMR spectra of **1** in d^8-THF at (a) 20 °C and (b) −80 °C.

Protons as well as Lewis bases also add to the two-electron mixed-valence core of **1**. Addition of neat triflic acid to suspensions of **1** in CH_2Cl_2 yields no appreciable reaction, even after 24 h; however, if the triflic acid is added as a solution in MeCN, rapid dissolution of the solid occurs to give a pale yellow, almost colorless solution from which a pale yellow solid may be isolated. The presence of a hydride ligand is revealed by the appearance of a Ir−H stretching mode at 2042 cm^{-1} in the infrared spectrum of the isolated product as well as a single low-frequency hydride resonance at −12.67 ppm (Figure 3a) in the ^1H NMR spectrum of the compound in CD_3CN. The

(59) Sola, E.; Navarro, J.; López, J. A.; Lahoz, F. J.; Oro, L. A.; Werner, H. *Organometallics* **1999**, *18*, 3534−3546.

(60) Jordan, R. B. *Reaction Mechanisms of Inorganic and Organometallic Systems*, 2nd ed.; Oxford University Press: New York, 1998.

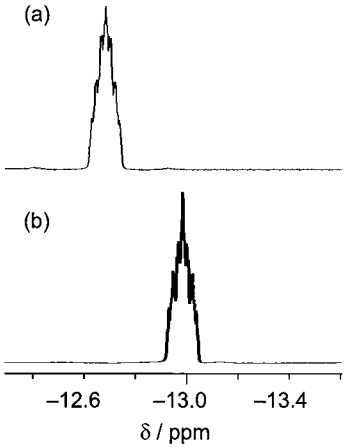

Figure 3. The low-frequency region of the ^{1}H NMR spectra that displays the complex *cis* $^2J_{P-H}$ coupling pattern for iridium hydride complexes (a) **4** and (b) **7a**.

absence of a large $^2J_{P-H}$ coupling in the low frequency resonance suggests only *cis* H,P interactions,[61] requiring protonation to occur at the axial coordination site of either the Ir^0 or Ir^{II} center. For either case, HOTf formally oxidizes the complex by two electrons. We postulate that H^+ adds to the axial position of the electron-rich Ir^0 center to give the $Ir^{I,III}$ complex $[HIr_2(tfepma)_3Cl_2(MeCN)]OTf$, **4**, where the chelating ligand is forced into the equatorial coordination plane.

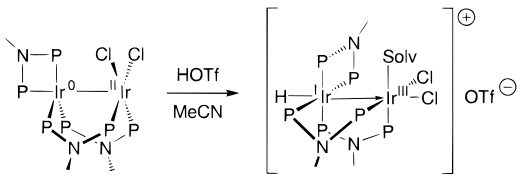

1 **4**

Our proposal for the protonation reaction is based on the following ^{1}H and ^{31}P NMR data (Supporting Information, Figure S2): (1) The ^{31}P NMR resonances of **4** at 53.63 and 66.90 ppm are in the range for phosphites at the Ir^{III} center of structurally characterized complexes **5** and **7b** (55−57 and 64−68 ppm, respectively). The difference in the two chemical shifts suggests that the phosphites are opposite to different ligands with the lower-frequency signal arising from the phosphite situated across from the ligand with the weaker *trans* influence.[62] A singlet resonance in the ^{1}H NMR spectrum at 2.59 ppm identifies this ligand as MeCN, which is coordinated to the Ir^{III}. Accordingly, the 53.63-ppm resonance is assigned to the phosphite *trans* to MeCN and the phosphite opposite the stronger coordinating chloride ligand is assigned to the 66.90-ppm resonance. (2) Two other sets of ^{31}P resonances for phosphites coordinated to Ir^I flank the Ir^{III} phosphite resonances to higher (75.93 and 84.95 ppm) and lower (43.01 and 48.38 ppm) frequencies. Similar trends are observed in the ^{31}P NMR spectra of other $Ir_2^{I,III}$ compounds **5**, **7b** and **8**. The low-frequency resonance is assigned to the chelating phosphite and the high-frequency resonance is assigned to the bridging phosphite (vide infra). (3) The large $^2J_{P-P}$ coupling constants (739 and 722 Hz and 744 and 716 Hz for the phosphite resonances of the bridging and chelating ligands, respectively) of these signals confirm a *trans* disposition of phosphite ligands in the equatorial plane of the Ir^I metal center. Consistent with this result, the ^{1}H methyl resonances of the two bridging ligands exhibit chemical shifts of 2.73 and 2.86, differing little from those of **1** and **3**, whereas that of the chelating ligand is shifted to higher frequency.

Akin to **3**, the MeCN of **4** undergoes solvent exchange. The disappearance of the coordinated MeCN signal is complemented by the appearance of a signal for uncoordinated MeCN at 1.96 ppm. The exchange process is sufficiently slow such that the loss in intensity of the ^{1}H resonance of the Ir^{III}-coordinated MeCN may be easily monitored over the course of a day. A plot of ln I vs t is linear ($R^2 = 0.9984$), yielding a first-order decay rate constant of $k_H = 1.25 \times 10^{-4}$ s^{-1}. As compared to **3**, the significantly smaller exchange rate constant is consistent with the 36 e$^-$ count of **4** and the inertness of its octahedral Ir^{III} center. Interestingly, the MeCN exchange process is significantly accelerated ($k_D = 1.90 \times 10^{-4}$ sec^{-1}, $R^2 = 0.9985$) when **1** is deuterated by DOTf. The measured inverse kinetic isotope effect of 0.66 is notable inasmuch as it indicates a strengthening of the Ir^I−H bond (as opposed to Ir^I−H bond cleavage) along the reaction pathway for MeCN exchange.[63] As indicated by a comparison of Ir^0−L_{ax} bond distances in the crystal structures of **1** vs **2a** and **3**, the axial ligand is more strongly coordinated when there is no other ligand along the metal−metal axis. On this basis, loss of the coordinated MeCN ligand followed by a rearrangement to square pyramidal geometry should lead to a stronger Ir−H/D bond, thus accounting for the inverse secondary isotope effect.

Oxidation Chemistry of the $Ir_2^{0,II}Cl_2$ Core. The oxidation−reduction chemistry of **1** with chlorine, hydrogen chloride, and hydrogen is summarized in Figure 4. Thermal ellipsoid plots are presented for selected products and accompanying metrical data are listed in Tables 1−3.

Chlorine, in the form of its iodobenzene adduct, readily adds to **1** to give the $Ir_2^{I,III}$ two-electron mixed-valence complex $Ir_2(tfepma)Cl_4$ (**5**). X-ray crystallographic analysis of **5** reveals that halogen addition occurs across the metal−metal bond, which is characterized by an Ir−Ir distance of 2.7765(8) Å (Table 2). Simple electron counting arguments are consistent with the formulation of an $Ir^I \rightarrow Ir^{III}$ dative bond in which both metals assume an octahedral coordination geometry. An average value of 32° for the twist angle of L_{eq}−Ir^I−Ir^{III}−L_{eq}' is close to the sterically preferred twist angle of 45° for the octahedral coordination spheres of two metals juxtaposed by a single bond.[64] The Ir^{III}−Cl bond distances for **5**, listed in Table 2, are noticeably longer than the corresponding Ir^{II}−Cl bonds of **1** and **3**. This result is peculiar in light of the anticipated contraction of the iridium radius upon oxidation of Ir^{II} to Ir^{III}. Iridium−phosphorus bond distances for the bridging ligands of **5** are unchanged from precursor **1**; however, the Ir−P distances associated with the chelating ligand elongate by ∼0.1 Å.

NMR spectra of **5** are consistent with the octahedral coordination geometry of the oxidized metal core. The distinct environments of a chelating and two bridging ligands are signified by ligand methyl resonances in the ^{1}H NMR spectrum at 2.71 ppm and 2.88 and 2.93 ppm, respectively. The ^{31}P{^{1}H} NMR spectrum of **5** (Supporting Information, Figure S2) consists of six separate resonances, one for each of the unique phosphites. P(3) and P(5) of **5** are expected to be strongly coupled owing to their *trans* arrangement. In this context, signals at 13.14 and 74.31 ppm are ascribed to P(5) and P(3),

(61) Kaesz, H. D.; Saillant, R. B. *Chem. Rev.* **1972**, *72*, 231−281.
(62) Crabtree, R. H. *The Organometallic Chemistry of the Transition Metals*; Wiley: New York, 1994.
(63) Lowry, T. H.; Schueller-Richardson, K. *Mechanism and Theory in Organic Chemistry*, 3rd ed.; Harper & Row: New York, 1987; pp 232−237.
(64) Albright, T. A.; Burdett, J. K.; Whangbo, M.-H. *Orbital Interactions in Chemistry*; Wiley-Interscience: New York, 1985.

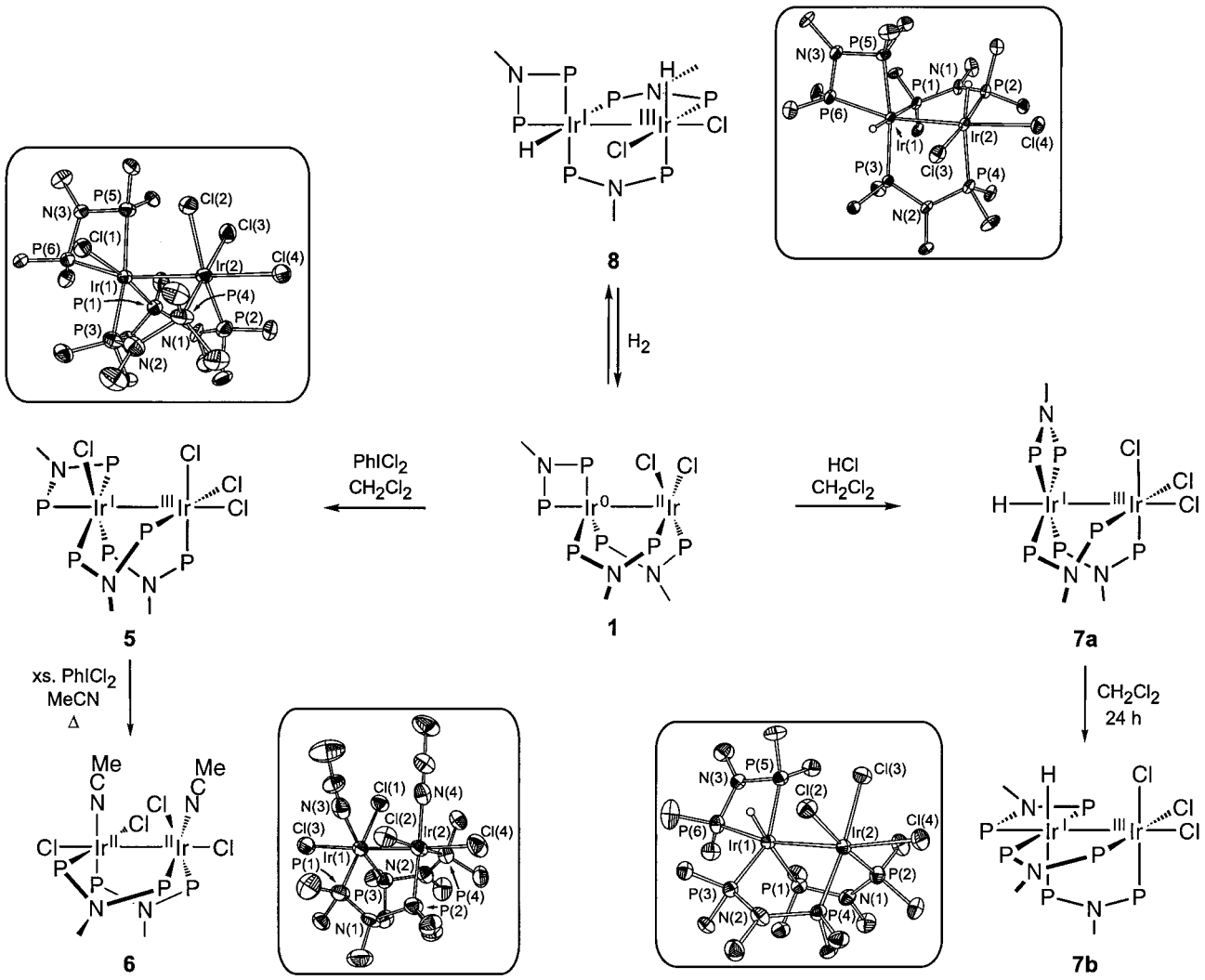

Figure 4. Oxidative-addition chemistry of $Ir_2(tfepma)_3Cl_2$ (**1**). Thermal ellipsoid plots of the crystal structures are drawn at the 50% probability level and the numbering scheme is shown. Solvent molecules and $-CH_2CF_3$ groups are omitted for clarity. In the case of **5** and **6**, only one of the two crystallographically unique molecules is presented.

respectively, based on a $^2J_{P-P}$ coupling constant of 901 Hz. As in $Ir_2^{0,II}$ complexes **1**−**3**, the low-frequency resonance at 9.24 ppm is attributed to the P(6) phosphite *trans* to the Ir−Ir bond. On the basis of the ^{31}P COSY spectrum of **5**, the 66.46-ppm resonance is ascribed to the Ir^I-bound P(1) phosphite of the bridging ligand, while the signals at 54.98 and 57.11 ppm are assigned to Ir^{III}-bound P(2) and P(4) phosphites of the bridging ligands, respectively.

Treatment of **5** with $PhICl_2$ in refluxing MeCN results in the loss of the chelating tfepma ligand, which is subsequently oxidized, preventing its incorporation back into the coordination sphere of the binuclear core. A bright yellow solid (**6**), possessing relatively simple NMR spectra, is obtained. The ^1H NMR spectrum comprises a single methyl resonance at 2.80 ppm and four methylene resonances between 4.48 and 5.46 ppm for the diphosphazane ligands. The ^1H NMR signal of CH_3CN is that of free ligand indicating that the bound solvent molecule is exchanged immediately upon dissolution of solid samples of the compound. The ^{31}P NMR spectrum of **6** exhibits two resonances at 54.97 and 57.87 ppm with a simple AA′BB′ coupling pattern. These NMR results point toward a symmetric complex, which is verified by X-ray diffraction studies on single crystals of **6**. Two bridging *cis*-diphosphazane ligands span a $Ir_2^{II,II}-Cl_4$ core, supporting octahedral coordination geometries that are related to each other by a 30° twist angle about the internuclear axis. A metal-metal bond distance of 2.7525(9) Å signifies a formal bonding interaction that is characteristic of a binuclear $(d^7)_2$ complex.[65−67] One chloride ligand is located *trans* to the Ir−Ir bond and another is located in the equatorial plane. Acetonitrile completes the octahedral coordination spheres of the metal centers. The Ir−P bond distances are in the expected range, as are the Ir−Cl bond distances, which are slightly shorter along the metal−metal bond axis. Other metrical parameters for **6** can be found in Table 3. The formation of **6** is in accord with our studies of dirhodium dfpma and tfepma complexes.[45,68] In these systems, as observed here, valence symmetric cores are obtained when two diphosphazane ligands span the core; the explicit stabilization of a two-electron mixed-valence core requires the presence of three diphosphazane ligands.

The lability of the acetonitrile ligands suggested to us that their displacement by a tfepma ligand would provide access to a symmetric $Ir_2^{II,II}Cl_4$ complex spanned by three bridging

(65) Jenkins, J. A.; Ennett, J. P.; Cowie, M. *Organometallics* **1988**, *7*, 1845−1853.

(66) Cotton, F. A.; Eagle, C. T.; Price, A. C. *Inorg. Chem.* **1988**, *27*, 4362−4368.

(67) Cotton, F. A.; Dunbar, K. R.; Verbruggen, M. G. *J. Am. Chem. Soc.* **1987**, *109*, 5498−5506.

(68) Heyduk, A. F.; Odom, A. L.; Nocera, D. G., to be published.

Table 2. Selected Crystallographic Bond Distances (Å) and Angles (deg) for the Complexes **5**, **7a**, and **8**[a]

	bond distances/Å		
	5[b]	**7b**[c]	**8**[d]
Ir(1)−Ir(2)	2.7765(8)	2.7775(11)	2.7561(7)
Ir(1)−X(1)	2.435(4)		
Ir(2)−Cl(2)	2.405(4)	2.450(2)	2.465(3)
Ir(2)−X(3)	2.428(4)	2.418(2)	
Ir(2)−Cl(4)	2.504(4)	2.487(2)	2.511(3)
Ir(1)−P(1)	2.223(4)	2.314(2)	2.300(3)
Ir(1)−P(3)	2.282(4)	2.241(2)	2.259(3)
Ir(1)−P(5)	2.375(4)	2.322(2)	2.271(3)
Ir(1)−P(6)	2.350(4)	2.269(2)	2.278(3)
Ir(2)−P(2)	2.198(4)	2.188(2)	2.160(3)
Ir(2)−P(4)	2.191(4)	2.175(2)	2.277(3)

	bond and torsion angles/deg		
	5[b]	**7b**[c]	**8**[d]
P(1)−Ir(1)−X(1)	173.3(2)		
P(1)−Ir(1)−P(3)	93.4(2)	100.60(8)	96.70(11)
P(1)−Ir(1)−P(5)	99.9(2)	103.61(7)	93.99(11)
P(2)−Ir(2)−P(4)	96.0(2)	94.05(8)	103.61(12)
P(2)−Ir(2)−Cl(2)	170.7(2)	175.14(7)	169.33(12)
P(2)−Ir(2)−X(3)	86.2(2)	89.13(8)	
P(6)−Ir(1)−Ir(2)	165.20(11)	167.41(6)	158.45(10)
Cl(4)−Ir(2)−Ir(1)	178.07(10)	171.62(5)	176.34(8)

	bond and torsion angles/deg		
	5[b]	**7b**[c]	**8**[d]
X(1)−Ir(1)−Ir(2)−Cl(2)	39.4	19.2	7.2
X(1)−Ir(1)−Ir(2)−Cl(2)	39.4	19.2	7.2
P(1)−Ir(1)−Ir(2)−P(2)	24.4	15.2	18.5
P(3)−Ir(1)−Ir(2)−P(4)	27.0	21.9	11.5
P(5)−Ir(1)−Ir(2)−X(3)	37.9	0.7	1.6

[a] Except where noted, X = Cl. The values tabulated for **5** are the average values for the two crystallographically different but chemically identical molecules in the asymmetric unit. [b] X(1) = X(3) = Cl for **5**. [c] X(1) = H and X(3) = Cl for **7b**. [d] X(1) = X(3) = H for **8**.

Table 3. Selected Crystallographic Bond Distances (Å) and Angles (deg) for **6**[a]

bond distances/Å		bond and torsion angles/deg	
Ir(1)−Ir(2)	2.7525(9)	P(1)−Ir(1)−P(3)	94.6(2)
Ir(1)−Cl(1)	2.434(5)	P(1)−Ir(1)−N(4)	94.4(4)
Ir(1)−Cl(3)	2.486(4)	P(1)−Ir(1)−Cl(1)	177.3(2)
Ir(1)−P(1)	2.205(5)	P(2)−Ir(2)−P(4)	94.5(2)
Ir(1)−P(3)	2.210(5)	P(2)−Ir(2)−Cl(2)	87.3(2)
Ir(1)−N(3)	2.093(17)	P(2)−Ir(2)−N(3)	173.3(5)
Ir(2)−Cl(2)	2.432(4)	Cl(3)−Ir(1)−Ir(2)	174.22(13)
Ir(2)−Cl(4)	2.468(4)	Cl(4)−Ir(2)−Ir(1)	176.15(12)
Ir(2)−P(2)	2.214(5)		
Ir(2)−P(4)	2.198(5)	Cl(1)−Ir(1)−Ir(2)−N(4)	32.2
Ir(2)−N(4)	2.06(2)	P(1)−Ir(1)−Ir(2)−P(2)	27.5
		P(3)−Ir(1)−Ir(2)−P(4)	27.3
		N(3)−Ir(1)−Ir(2)−Cl(2)	34.6

[a] The tabulated values are averages for the two crystallographically different but chemically identical molecules in the asymmetric unit.

ligands, similar to that observed for Rh_2 dfpma chemistry.[33,45] Addition of one equivalent of tfepma to solutions of **6** in CH_2Cl_2, however, leads to nearly quantitative (> 90%) conversion to the $Ir_2^{I,III}$ complex, **5**, as determined with $^{31}P\{^1H\}$ NMR spectroscopy. The prevalence of **5** is noteworthy. In the absence of a scavenger (e.g., $PhICl_2$) of free tfepma, **5** is recovered quantitatively from refluxing acetonitrile with no evidence for the formation of **6**.

The reaction of **1** with HCl produces a $Ir_2^{I,III}$ product analyzing as $Ir_2(tfepma)_3HCl_3$ (**7b**). An Ir−H stretch in the IR spectrum at 2115 cm^{-1} is consistent with a terminal hydride ligand situated *trans* to a phosphite.[61] Figure 5a displays the single hydride resonance observed in the ^1H NMR spectrum of **7b**. The large 178-Hz $^2J_{P-H}$ coupling constant for this signal at −10.24 ppm provides further support for a *trans* H,P arrangement. A signal in the ^{31}P NMR spectrum (Figure S2, Supporting Information) at 86.40 ppm was identified by $^{31}P-^1H$ HMQC experiments to correspond to the Ir^I phosphite coordinated *trans* to the hydride. The high-frequency shift of this resonance is consistent with the strong *trans* influence of the hydride ligand.[62] The conspicuously vacant site in the X-ray crystal structure of **7b** (Figure 4) confirms the location of the hydride in the equatorial plane of the Ir^I center. Moreover, after the location of all non-hydrogen atoms, the Fourier difference map showed a single peak in the vacant iridium coordination site of appropriate intensity for a hydride ligand, though the proximity of the hydride to a heavy nucleus precludes the determination of an accurate Ir−H distance. The strong *trans* influence of the hydride ligand is apparent from a Ir(1)−P(1) bond distance in **7b** that is 0.091(3) Å longer than that Ir(1)−P(1) bond distance of chloride analogue **5** (d(Ir(1)−P(1)) = 2.314(2) Å in **7b** vs 2.223(4) Å in **5**). Excluding Ir(1)−P(1), all other metal−ligand bond distances of **7b** are similar to those observed in **5** (Table 2). The Ir−Ir bond distance of 2.7775(11) Å is in the standard range. The 14° average twist angle about the metal−metal axis poises the iridium complex in a nearly eclipsed conformation. The three different tfepma ligand environments displayed in the crystal structure of **7b** are distinguished in the ^1H NMR spectrum by unique methyl resonances at 2.65, 2.77, and 2.89 ppm. Two resonances at 64.38 and 67.79 ppm in the $^{31}P\{^1H\}$ NMR spectrum are assigned to Ir^{III} phosphites, whereas the low frequency singlet at 21.64 ppm is assigned to the axially coordinated phosphite of the chelating ligand. As in **5**, a strong $^2J_{P-P}$ of 761 Hz for resonances at 26.61 and 82.15 ppm is in accordance with a *trans* arrangement of Ir^I-coordinated phosphites from the chelating and bridging ligands, respectively.

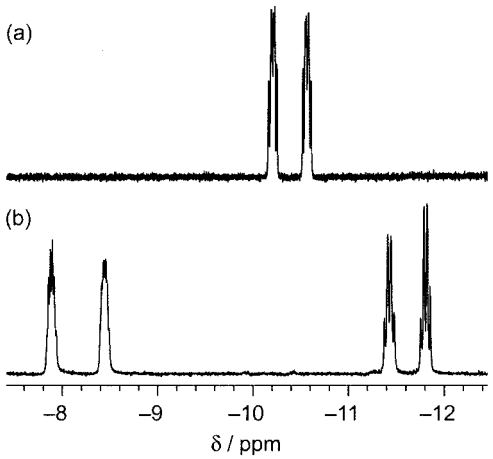

Figure 5. The low-frequency region excised from the ^1H NMR spectra (CD_3CN) of iridium hydride complexes (a) **7b** and (b) **8**. The location of a hydride ligand *trans* to a phosphorus atom is easily distinguished by the strong $^2J_{P-H}$ coupling pattern.

The formation of **7b** is preceded by a compound that can be isolated as a solid of the same empirical formula during the early stages of the reaction between HCl and **1**. Indeed, as implied in the reaction pathway of Figure 4, this precursor complex converts to **7b** upon stirring in CH_2Cl_2. Examination of the Ir-stretching region of the IR spectrum gives a single stretch at 2037 cm^{-1}, and the ^1H NMR spectrum shows a single hydride resonance at −13.0 ppm, exhibiting only *cis* $^2J_{P-H}$ couplings. As shown in Figure 3, the similarity of the NMR

signatures of this hydride product to that of **4** leads us to propose isomer **7a** (Figure 4), possessing the hydride in the axial position of Ir^{I} and the chelating phosphite rotated into the equatorial plane. In support of this contention, the ^{31}P NMR spectrum of **7a** is also nearly identical to that of **4**. Signals of the chelating phosphite at 35.71 and 47.88 ppm show strong $^{2}J_{P-P}$ couplings of 795 and 752 Hz. Moreover, the chemical shifts of the bridging phosphites of the Ir^{I} (88.80 and 88.66 ppm) and Ir^{III} (63.79 and 66.34 ppm) centers are consistent with those observed in **4**.

Reversible Addition of H_2 to 1. Brown CH_2Cl_2-solutions of **1** rapidly turn pale yellow upon bubbling with hydrogen gas at room temperature and then back to brown with N_2 purging. Two iridium−hydride resonances in the low-frequency region of the ^{1}H NMR spectrum at −11.51 and −8.32 ppm attend the appearance of the yellow solution. As shown in Figure 5b, large $^{2}J_{P-H}$ coupling constants distinguish these resonances. The 172-Hz coupling constant of the lower frequency peak is commensurate with the 178-Hz coupling constant observed for the Ir^{I} hydride in **7b**. An even larger $^{2}J_{P-H}$ coupling constant of 270 Hz for the −8.32 ppm resonance points toward a *trans* H,P arrangement at the Ir^{III} center; the contracted radius of the oxidized metal center accounts for this large coupling constant.[61] Oxidative-addition of hydrogen across the diiridium bond to give a $HIr^{I}\rightarrow Ir^{III}Cl_2H$ core is confirmed by the X-ray crystal structure of the dihydride product (**8**) shown in Figure 4; selected bond distances and angles are presented in Table 2. Although the Ir^{III}-coordinated hydride could not reliably be located (only the Ir^{I}-coordinated hydride could be located in the difference Fourier map), two large void spaces in the octahedral ligand spheres establish the location of each hydride. Furthermore, a substantial increase in Ir(1)−P(1) and Ir(2)−P(4) bond distances relative to **5** is in accord with the location of the P(1) and P(4) phosphites *trans* to the terminal hydride ligands. The average twist angle about the Ir−Ir bond axis is only 10°; the H(1)−Ir(1)−Ir(2)−H(2) dihedral angle in the solid state is 88°. The diiridium bond distance is significantly shorter than in $Ir_2^{I,III}$ complexes **5** and **7b**, and in fact is more comparable to the bond distance observed in the $Ir_2^{II,II}$ complex, **6** (d (Ir(1)−Ir(2)) = 2.7525(9) Å as compared to 2.7561(7) Å in **8**). Other metrical parameters of **8** are largely unchanged from those of complexes **5** and **7b**.

The $^{31}P\{^{1}H\}$ NMR spectrum of **8** shows a six resonance pattern similar to those observed for complexes **5** and **7b**. The chelating ligand resonances appear shifted to low frequency as a doublet-of-triplets at 17.85 ppm and a strongly coupled doublet at 45.26 ppm ($^{2}J_{P-P}$ = 750 Hz). This 750 Hz coupling constant is also observed in a resonance at 95.50 ppm, easily identifying this resonance as an Ir^{I}-phosphite from a bridging tfepma ligand. $^{31}P-^{1}H$ HMQC experiments allowed for the correlation of the ^{31}P NMR resonances at 86.84 and 99.40 ppm to the Ir^{I} and Ir^{III}-coordinated hydrides, respectively. A peak at 71.34 ppm is assigned to an Ir^{III} phosphite, located *trans* to a chloride ligand.

Discussion

The stabilization of an $Ir_2^{0,II}$ core with bidentate diphosphazanes concurs with lessons learned from the structural chemistry of Rh_2 dfpma complexes. Tolman's steric and electronic correlation for phosphines[69] establishes $P(OR)_2$ to be of comparable π-acidity to PF_2. The framework of bidentate diphosphazanes therefore preserves the crucial feature of an electron lone pair on a bridgehead atom juxtaposed to π-accepting orbitals of atoms bonded directly to the metal. As we observe in Rh_2 dfpma chemistry, a ligand architecture possessing such stereoelectronic properties predisposes bimetallic cores to internally disproportionate; the $Ir^{I}(\mu\text{-}X)_2Ir^{I}$ core, which typifies diiridium chemistry,[70] is observed only as a transient along the reaction pathway to **1**. Moreover, the tfepma ligand provides the additional flexibility of tuning the ligand's electronic and steric properties with R substitution on the phosphite, factors crucial to the two-electron mixed-valence chemistry of iridium. Along these lines, the dfpma ligand does not provide access to the mixed-valence diiridium cores reported here. Unlike the trifluorethoxy substituents of tfepma, the fluorines of dfpma are too small to protect the diridium core from oligomerization, thus subverting the isolation of molecular $Ir_2^{0,II}$ compounds.

The constraints imposed by the bulky trifluoroethoxy groups are readily apparent in the crystal structure of **1**. Sufficient steric clashing of the trifluoroethoxy groups forms a sculpted pocket at the 16 e^- coordinatively unsaturated Ir^{II} center into which two-electron donor ligands are readily received, as exemplified by **2a**−**c**. Perfunctory steric considerations also appear to explain the peculiar asymmetric coordination of the $Ir_2^{0,II}$ core by one chelating and two bridging tfepma ligands, a structural departure from Rh_2 dfpma chemistry. Yet three diphosphzane ligands span the smaller $Rh_2^{II,II}$ core of $Rh_2(tfepma)_3Cl_4$,[45] suggesting that there is enough room to bridge three diphosphazanes about an $Ir_2^{0,II}$ bimetallic center. Our inability to simply substitute the CH_3CN ligands of **6**, exclusive of rearrangement to **5**, suggests a thermodynamic persistence for the chelating tfepma ligand.

Reducible substrates effectively add across the metal−metal bond of **1** to produce $Ir_2^{I,III}$ addition products. Coordinative unsaturation at the Ir^{II} center is paramount to the reactivity of **1** as supported by the inertness of **2a**−**c** to the same substrates. For example, whereas $PhICl_2$ immediately reacts with **1** to give **5**, the conversion of **2a**−**c** to of **5** proceeds to only 10% after 24 h. This arrested reactivity of **2** suggests that ligand dissociation, which is slow for coordinatively saturated 36 e^- complexes, must precede oxidative addition. Similarly, the $Ir_2^{I,III}$ addition products of Figure 4 are averse to further oxidation, a result of their 36 e^- count and the coordinative saturation attendant with the octahedral ligand spheres of both metal centers. The aforementioned stability of **5** to $PhICl_2$ is the most striking example of this retarded reactivity of the $Ir_2^{I,III}$ core, and is entirely in accordance with the chemistry of square planar M^{I} (square planar)$\rightarrow M^{III}$ (octahedral) (M = Rh and Ir) complexes. As revealed in Halpern's meticulous kinetics studies,[71] the formation of a robust and unreactive $Rh_2^{I,III}$ mixed-valence complex poisons Wilkinson's catalytic cycle. Only when the 36 e^- dative $M^{I}\rightarrow M^{III}$ bond is exposed to the incoming electrophile, as in the open boat structure of $Rh_2^{I,III}$ pyrazolate complexes,[36,37] does oxidative addition become a viable reactivity pathway.

Molecular orbital calculations are consistent with the reaction chemistry displayed in Figure 4. Extended Hückel calculations of the frontier molecular orbitals for the idealized $Ir_2(PH_3)_6Cl_2$ complex are shown in Figure 6. Bearing a striking resemblance to the frontier orbital set of the previously reported d^7-d^9 mixed-valence rhodium complexes,[34] a LUMO of principally $d\sigma^*$ parentage is energetically proximate to a HOMO of mixed $d\pi/d\delta$ character. The low-energy placement of the LUMO results from the absence of an axial ligand coordinating the Ir^{II} center. This unoccupied, energetically accessible, orbital is ideally suited to receive two-electron donor ligands. Destabilization of the LUMO provides the energetic recompensation for the formation the two-electron $Ir^{II}-L_{ax}$ bond in the reaction of **1** to **2**. The

(69) Tolman, C. A. *Chem. Rev.* **1977**, *77*, 313−348.

(70) Serpone, N.; Jamieson, M. A. In *Comprehensive Coordination Chemistry*; Wilkinson, G., Gillard, R. D., McCleverty, J. A., Eds.; Permagon: Oxford, 1987; Vol. 4, pp 1097−1178.

(71) Halpern, J. *Inorg. Chim. Acta* **1982**, *62*, 31−37.

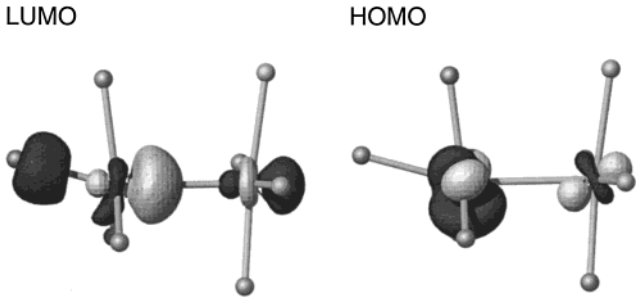

Figure 6. Pictorial representation of the HOMO and LUMO of $Ir_2(PH_3)_6Cl_2$ as calculated by the extended Hückel program YAeHMOP. Bond lengths and angles taken from the crystal structure of **1** were used to define the metal coordination environment.

LUMO also governs the oxidation-addition chemistry of the $Ir_2^{0,II}$ core. Oxidative addition of small molecule substrates to **1** leads to occupation of the vacant axial site. Again, significant destabilization of the LUMO attends the formation of the ligand-centered bonding orbitals.

The ability of the tfepma ligand to be sufficiently flexible to support the variant coordination geometries and correspondent electronic structures of the two-electron mixed-valence cores is crucial to the reactivity of Figure 4. In one-electron mixed-valence compounds, a single electron change can be accommodated with an inflexible coordination sphere. However, this is unlikely to be the case for two-electron mixed-valence species. Significant changes in the reorganization of the primary coordination environment must typically accompany the addition or removal of more than one electron from a metal center. As Bosnich postulates in his studies of 6−4 binucleating complexes,[72,73] this ligand reorganization or "mechanical coupling" between metal centers is likely the origin for the arrested multielectron redox reactivity of mixed-valence complexes. In **1**, adverse energetics associated with mechanical coupling are circumvented by the flexible coordination environment offered by the tfepma ligands. The three atom PNP backbone can support twist angles from 0 to 45°, thus permitting the preferred trigonal bipyramidal and octahedral coordination geometries of d^9 and d^7 metal centers, respectively, to be adopted with facility upon oxidative-addition to the $Ir_2^{0,II}$ bimetallic core.

The proclivity of the two-electron mixed-valence diirdium platform to support hydrides, formed along simple acid−base or oxidative-addition reaction pathways, is a particularly intriguing result of Figure 4. For reactions with acid, the hydride is accommodated at the electron rich, low-valent iridium center. The facility at which proton transfer occurs is striking when compared to the reactivity of symmetric $Ir_2^{I,I}$ cores, which are seldom protonated by HCl.[74,75] The reactivity of **1** is undoubtedly a result of the greater basicity of the Ir^0 center of a mixed-valence bimetallic core as compared to that of a symmetric Ir^I binuclear center. The formation of **7a** and its subsequent isomerization to **7b** suggests that the proton initially transfers to the axial position of Ir^0 center, *trans* to the metal−metal bond. Further confirmation for initial proton transfer to the axial site of Ir^0 comes from the reaction of **1** with the protons of weakly coordinating anions such as HOTf to produce **4**. A suitable coordinating ligand such as MeCN is needed to stabilize the hydride. In the absence of a coordinating ligand, proton transfer does not occur and the $Ir_2^{I,III}$ product is not observed, suggesting that either ligand coordination precedes protonation or that a concerted addition mechanism is operative. In the case of HCl, Cl^- is the coordinating ligand that drives proton addition to the $Ir_2^{0,II}$ core.

Two-electron mixed-valence hydrides are also produced by the direct reaction of **1** with hydrogen. As in **7b**, vacant octahedral coordination sites in the X-ray crystal structure of **8** and large $^2J_{P-H}$ coupling constants are signatures of the hydride ligands. The reversible addition of H_2 to **1** and its elimination from **8** is an unusual and intriguing result because there are relatively few examples of reversible H_2 addition across metal−metal bonds, and to our knowledge,[76−78] in no case, has such a reaction been observed to occur reversibly across a preserved metal−metal single bond.[79] Initial attempts to use para hydrogen to probe the addition mechanism[80] have been unfruitful, a likely result of slow H_2 exchange between the complex and para-enriched hydrogen. However, the results of the variable temperature NMR studies of the solvent exchange process involving **1** and **3** provide some insights into the H_2 addition mechanism. The equivalence of the Ir^{II}-coordinated phosphites in the fast exchange regime requires a common intermediate through which the two phosphites may permute. An exchange process, consistent with both NMR and X-ray crystallographic results, is as follows.

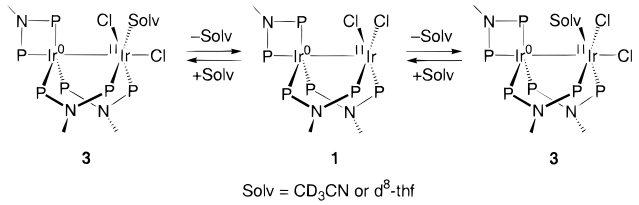

With the understanding that weak 2 e^- donor ligands occupy an equatorial site of the Ir^{II} coordination sphere, this metal center provides a logical site for H_2 activation. Conversion to the dihydride may occur according to the following reaction sequence.

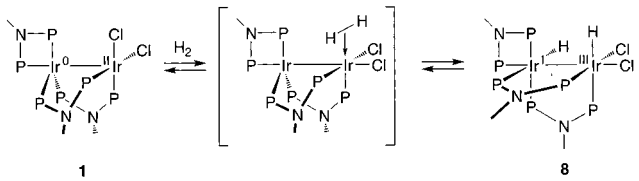

Single-site addition to the binuclear core[81] followed by hydride migration to produce the 1,2-dihydride[82] has been observed previously by Poilblanc and Cowie.[83−85] The alternative concerted 1,2 addition of H_2 across a metal−metal bond is forbidden by orbital symmetry considerations, as is the reverse,

(72) McCollum, D. G.; Bosnich, B. *Inorg. Chim. Acta* **1998**, *270*, 13−19.
(73) Bosnich, B. *Inorg. Chem.* **1999**, *38*, 2554−2562.
(74) Heinekey, D. M.; Fine, D. A.; Barnhart, D. *Organometallics* **1997**, *16*, 2530−2538.
(75) McDonald, R.; Sutherland, B. R.; Cowie, M. *Inorg. Chem.* **1987**, *26*, 3333−3339.
(76) Green, M. L. H.; Mountford, P. *Chem. Commun.* **1989**, 732−734.
(77) Qian, F.; Ferrer, M.; Green, M. L. H.; Mountford, P.; Mtetwa, V. S. B.; Prout, K. *J. Chem. Soc., Dalton Trans.* **1991**, 1397−1406.
(78) Safarowic, F. J.; Bierdeman, D. J.; Keister, J. B. *J. Am. Chem. Soc.* **1996**, *118*, 11805−11812.
(79) Hydrogen reversibly adds across the metal−metal bond of dirhodium porphyrins, but the Rh−Rh bond is cleaved. See for example: Zhang, X. X.; Wayland, B. B. *J. Am. Chem. Soc.* **1994**, *116*, 7897−7898.
(80) Eisenberg, R. *Acc. Chem. Res.* **1991**, *24*, 110−116.
(81) Hampton, C.; Cullen, W. R.; James, B. R.; Charland, J.-P. *J. Am. Chem. Soc.* **1988**, *110*, 6918−6919.
(82) Branchadell, V.; Dedieu, A. *New J. Chem.* **1988**, *12*, 443−453.
(83) Poilblanc, R. *Inorg. Chim. Acta* **1982**, *62*, 75−86.
(84) Guilmet, E.; Maisonnat, A.; Poilblanc, R. *Organometallics* **1983**, *2*, 1123−1127.
(85) Vaartstra, B. A.; Cowie, M. *Inorg. Chem.* **1989**, *28*, 3138−3147.

reductive elimination.[86] Pre-coordination of dihydrogen at Ir^{II} is further supported by the empirical observation that the rate of H_2 addition to **8** decreases with donor ability of the solvent, that is, CH_2Cl_2 > THF > MeCN. Presumably, CH_2Cl_2 cannot compete with H_2 as a sufficient donor ligand, whereas THF and MeCN show progressively higher Ir-solvent bond dissociation energies, slowing the addition of H_2 to **1**.

Accepting that H_2 addition proceeds via a single metal center, its reversible addition and elimination demands the formation of a two-electron mixed-valence species.

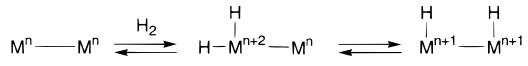

If the dihydride remains on one metal center, reversible H_2 elimination may be observed.[71,87−89] However, exclusive of the chemistry reported here, elimination is not reversible upon 1,2-dihydride rearrangement. In these cases, with the inability of most ligand systems to adequately support the formation of two-electron mixed-valence dihydrides, the overall process represented by eq 4 is disfavored. Conversely, in cases where a ligand system such as tfepma sustains two-electron mixed-valency, the reversible addition and elimination of H_2 may proceed smoothly through the dihydride as depicted in eq 4. Accordingly, in contrast to symmetric binuclear metal complexes, the reversible addition and elimination of H_2 to two-electron mixed-valence compounds may be another benchmark of the unique reactivity offered by two-electron mixed-valence compounds.

Concluding Remarks

A binuclear $Ir_2^{0,II}$ diphosphazane complex permits the systematic investigation of the oxidation−reduction chemistry of a two-electron mixed-valence core. The new reactivity of two-electron mixed-valence complexes described herein dovetails explicitly with our interest in defining new precepts for catalytic photoredox cycles relying on the multielectron activation of substrates in homogeneous solution. An important result of the chemistry depicted in Figure 4 is the facility at which H_2 is eliminated from a two-electron mixed-valence core. In typical HX energy conversion schemes, the photon is usually consumed in H_2 production[90−92] even though this reduction is the least energetically demanding component of the overall HX splitting cycle. It is, instead, X_2 elimination that is of greater thermodynamic pertinence owing to the high stabilities of the metal−halide bond. Indeed, the HX photochemistry of earlier investigations has been stoichiometric because the cycle to regenerate the initial photoreagent terminates with the formation of the metal dihalide.[47−49] For these reasons, we believe it imperative to develop a photoreagent from which H_2 production is facile, leaving the photon to effect the more thermodynamically challenging task of X_2 elimination. The weaker strength of Rh−H bonds compared to that of their Ir−H counterparts presages an even more active H_2 elimination chemistry from $Rh_2^{0,II}$ cores, an especially enticing prospect when considered in connection with our recent success in inducing the efficient photoelimination of X_2 via excitation of the metal localized excited states of $Rh_2^{0,II}$ complexes. Current studies are aimed at driving thermal H_2 and photochemical X_2 elimination from a single $Rh_2^{0,II}$ platform.

Acknowledgment. We thank Dr. Aaron Odom for helpful discussions, Dr. Jeff Simpson for his assistance with various 2D-NMR techniques, and Dr. William Davis for his help with X-ray crystal structure solutions. The National Science Foundation (Grant CHE-9817851) funded this research.

Supporting Information Available: ^{31}P NMR spectra of **1**, **2a**−**c**, **4**, **5**, and **7a**,**b**; input files for YAeHMOP calculations; ORTEP representations, tables of crystal data, atomic coordinates, bond lengths and angles, anisotropic thermal parameters, and hydrogen coordinates for compounds **3**, **5**, **6**, **7a**, and **8** (PDF). An X-ray crystallographic file, in CIF format. This material is available free of charge via the Internet at http://pubs.acs.org.

JA001491Q

(86) Trinquier, G.; Hoffmann, R. *Organometallics* **1984**, *3*, 370−380.
(87) Halpern, J.; Wong, C. S. *Chem. Commun.* **1973**, 629−630.
(88) Tolman, C. A.; Meakin, P. Z.; Lindner, D. L.; Jesson, J. P. *J. Am. Chem. Soc.* **1974**, *96*, 2762−2774
(89) Hampton, C.; Cullen, W. R.; James, B. R.; Charland, J.-P. *J. Am. Chem. Soc.* **1988**, *110*, 6918−6919.
(90) Balzani, V.; Carassiti, V. *Photochemistry of Coordination Compounds*; Academic Press: New York, 1970.
(91) Mann, K. R.; Lewin, N. S.; Miskowski, V. M.; Erwin, D. K.; Hammond, G. S.; Gray, H. B. *J. Am. Chem. Soc.* **1977**, *99*, 5525−5527.
(92) Trogler, W. C.; Erwin, D. K.; Geoffrey, G. L.; Gray, H. B. *J. Am. Chem. Soc.* **1978**, *100*, 1160−1163.